Progress In Electromagnetics Research C, Vol. 83, 33–44, 2018

Beam Focusing Compact Wideband Antenna Loaded with Mu-Negative Metamaterial for Wireless LAN Application

Sourav Roy*, Krishna L. Baishnab, and Ujjal Chakraborty

Abstract—This article proposes a beam focusing compact wideband microstrip antenna loaded with mu-negative (MNG) metamaterials. The antenna is designed to operate in the frequency spectra of IEEE 802.11a wireless LAN 5.15–5.85 GHz. The controlling of the beam direction has been investigated using eight different switching combinations of 12 PIN diodes which are integrated in the metamaterial unit cells. The main beam is found to be focused in $-ve\,y$, $+ve\,y$ and omnidirectional in yz plane in agreement with switching condition of the metamaterial unit cell. The maximum gain enhancement of 7 dB is obtained at 4.9 GHz in the negative y direction. The basic antenna with patch dimension $(0.14\lambda \times 0.14\lambda)$ provides wide fractional bandwidth of about 40%. Two prototypes of basic and proposed antennas have been developed using a low profile FR-4 substrate. The simulation results are found in good agreement with the measurement ones.

1. INTRODUCTION

Beam tilting technique has been effectively introduced to reduce the co-channel interference of antennas. It enhances transmission quality and increases the channel capacity of a communication system. In some previous related works, beam switching has been achieved either electronically or mechanically. Electronic beam switching is achieved by using RF Micro-Electro-Mechanical Systems (MEMS) switches or PIN diodes [1–3]. However, the antenna gain is found decreased due to scan loss. On the other hand, in mechanical controlling, gain performance of the antenna is not affected, but it increases the design cost, complexity and installation difficulty of the design.

Metamaterial is an artificial structure that exhibits unusual electromagnetic properties. It is widely used in different applications areas, such as sensors [4, 5], energy harvesting [6], wave polarization [7, 8], and controllable absorber [9]. It is also used for antennas performance enhancement, such as radiation enhancement [10], multi-directional beam generation [11], beam tilting [12–14], gain enhancement [15, 17], bandwidth enhancement [15], directivity [16], and multiband operation [18]. In [4], a circular split ring resonator based on metamaterial, used for fluid, strain and rotation sensing applications. In that resonator, a small variation of dielectric permittivity and loss tangent of the material and gap location results in variations of the resonance frequency. Metamaterial can prevents transmission or reflection of electromagnetic waves. The capability of absorption facilitates metamaterial used for energy harvesting [6] and controllable absorber [9] applications. The artificial structure element also plays a key factor to manipulate the orientation of the wave polarization. In [7], a meta-surface structure that is used as left- or right-hand circular wave polarizer designed simply by changing the orientation of the diagonal transmission line, and a novel EBG structure is designed for surface wave minimization which enhances radiation pattern of the low profile antenna presented in [10]. In [11], a metamaterial-based E-plane horn antenna is presented which radiates four directional beam patterns due to the extraordinary wave propagating phenomena of the metamaterial. A pattern controlled frequency tunable microstrip antenna loaded with multiple split ring resonators using RF MEMS switches is

Received 29 January 2018, Accepted 20 March 2018, Scheduled 8 April 2018
* Corresponding author: Sourav Roy (sourav31roy@gmail.com).
The authors are with the Department of ECE, N.I.T. Silchar, Assam, India.

presented to control the direction of the major lobe of the radiation pattern [12]. In [13], it is investigated that the integrated metamaterial loaded in a planar antenna can deflect the beam of an end-fire antenna by 17° with respect to the end-fire direction in the frequency range of 7.3–7.5 GHz. An electronic band-gap structure integrated with the orthogonal plane of a dipole antenna [14] is presented for tilting the beam about 28° at 3.5 GHz. The structure of the antenna is simple; however, the design complexity has increased the cost of the antenna.

In this paper, a compact wideband antenna is designed to operate in WLAN band. Split Ring Resonator (SRR) unit cells with PIN diode switching combinations are integrated into the patch and ground surface of the antenna substrate to investigate the radiation pattern characteristics. Due to the unique metamaterial properties, antenna beam is found to be tilted or focused in the $-y$ direction, $+y$ direction and omnidirectional in yz plane respectively for the particular switching combination which also influence the variation of the antenna gain in a particular direction. A prototype integrated with metamaterials has been designed, fabricated and measured, and found to be operated in the frequency spectra from 4.3 to 5.9 GHz.

2. BASIC ANTENNA DESIGN

A compact wideband antenna is designed on a commercially available low-cost FR-4 substrate with a dielectric constant of 4.4, thickness of 1.6 mm and loss tangent of 0.02. The overall dimension of the compact antenna (Antenna 1) is $19.6 \times 17\,\text{mm}^2$. A modified split ring resonator is used as the radiating patch. The maximum dimension of radiator is $7.5 \times 7.5\,\text{mm}^2$. The top view, side view and modified ground plane of the antenna with different parameters are shown in Fig. 1. The values of the different antenna parameters are mentioned in Table 1.

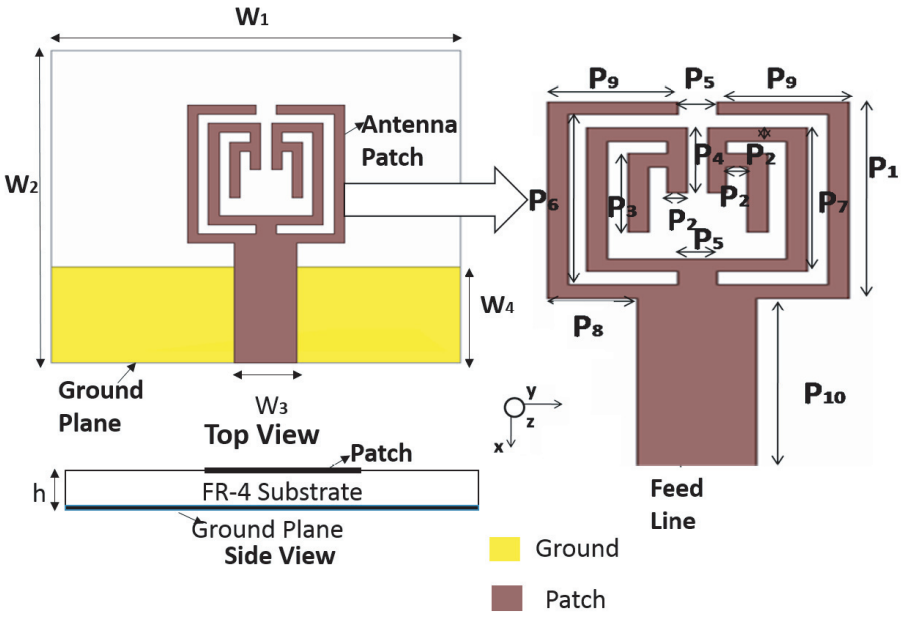

Figure 1. Geometry of Antenna 1.

Table 1. Antenna parameters.

Dimension	W_1	W_2	W_3	W_4	W_5	G_1	G_2	G_3	G_4	G_5	G_6
Length (mm)	19.6	17	3	5.2	3	2.3	0.3	2.05	4.2	1.05	0.5
Dimension	P_1	P_2	P_3	P_4	P_5	P_6	P_7	P_8	P_9	P_{10}	
Length (mm)	7.5	0.5	3	2.5	1	6.5	5.5	2.25	3.25	6.5	

3. BASIC ANTENNA RESULTS

The simulated and measured S_{11} (dB) plot of Antenna 1 and its fabricated prototype are shown in Fig. 2(a). The simulated and measured -10 dB bandwidths of Antenna 1 are 4.1 to 7.8 GHz and 4.2 to 7.2 GHz, respectively. The simulated and measured gains vs frequency plot are shown in Fig. 2(b). The measured gains of Antenna 1 at 5.2 and 5.8 GHz is 1.2 dB and 3 dB, respectively. The simulated result shows good agreement with measured one.

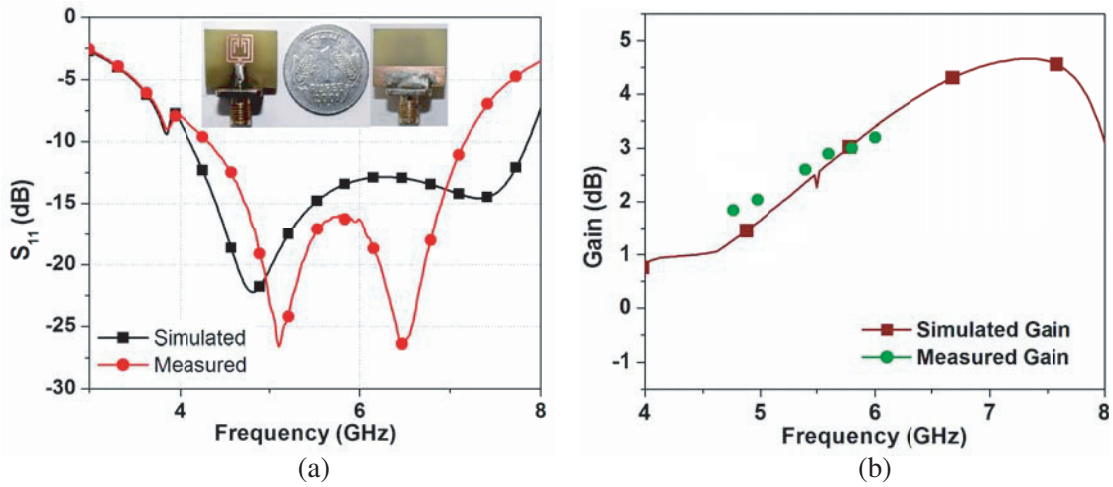

Figure 2. (a) Simulated and measured S_{11} parameter of Antenna 1 and (b) simulated and measured gain vs. frequency plot of Antenna 1.

It is found that the frequency spectrum depends on the antenna ground width (W_4) and substrate materials. The variation of S_{11} (dB) for different values of W_4 and substrate is shown in Figs. 3(a) and 3(b). Fig. 3(a) illustrates that Antenna 1 provides wide impedance bandwidth for $W_4 = 5.2$ mm. The lower frequency of Antenna 1 with different substrates is found almost the same; however, the upper frequency and bandwidth gradually increase with higher value of the substrate permittivity. Antenna gain is also found decreased due to higher dielectric loss of the higher permittivity substrates. For better realization, the effects of different substrates are compared and analyzed in Table 2. The low cost FR-4 substrate is found as a suitable choice for the design of WLAN antenna with the compact Antenna 1 configuration.

Table 2. Different substrate analysis.

Substrate Name	Relative Permittivity	Dielectric loss tangent	Substrate Thickness	Frequency Spectra	
				1st Band	2nd Band
Teflon (tm)	2.1	0.001	1.6 mm	4.15–5.05	5.10–10.02
RT-Duroid	2.2	0.0009	1.6 mm	4.13–4.95	5.01–9.63
Taconi TLE (tm)	2.95	0.0028	1.6 mm	4.1–4.53	4.59–9.06
FR-4	4.4	0.02	1.6 mm	4.11–7.84	9.33–10.91
Glass	5.5	0	1.6 mm	4.02–7.01	8.56–9.97
Taconic rf 60 (tm)	6.15	0.0028	1.6 mm	4.0–6.66	8.2–9.65

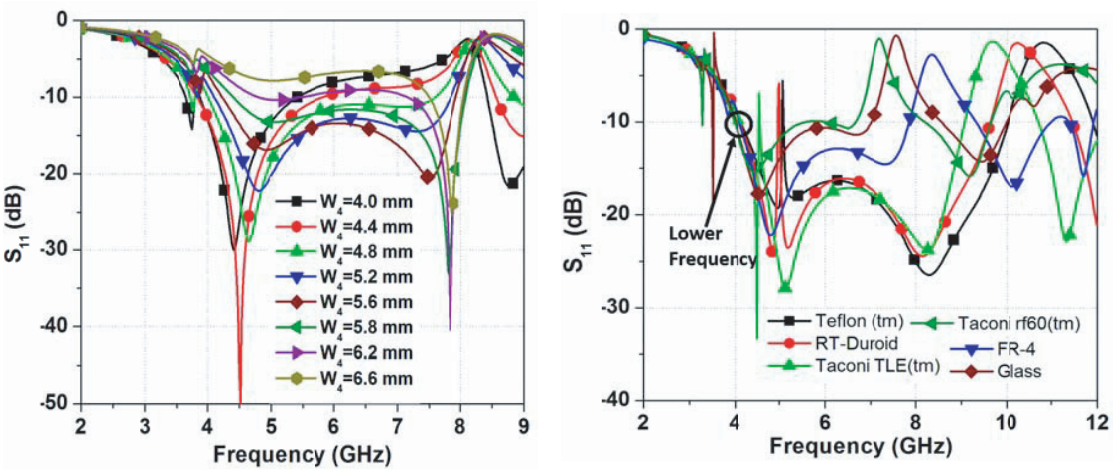

(a) (b)

Figure 3. (a) Simulated S_{11} parameter of antenna with variable W_4 and (b) simulated S_{11} parameter with different substrate material.

4. METAMATERIAL UNIT CELL

The SRR structure based on MNG metamaterial is shown in Fig. 4(a). The effective inductance and capacitance of the SRR structure, shown in Fig. 4(b), generate the resonance of the metamaterial structure.

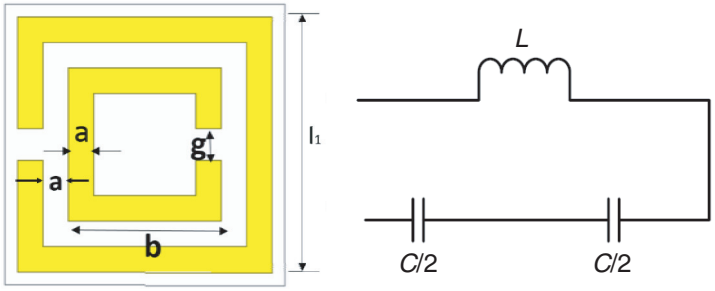

(a) (b)

Figure 4. (a) The geometry of the square split ring resonator metamaterial unit cell and (b) equivalent circuit representation of the SRR (C = capacitor, L = inductor).

The gap between two rings creates capacitive effect, and the length of resonator creates inductive effect. The approximated self-inductance per unit length of the two rings is given in Eq. (1) [15].

$$L = \left(\frac{\mu_0 b}{\sqrt{\pi}}\right)\left(\log\left(\frac{32b}{a\sqrt{\pi}}\right) - 2\right) \tag{1}$$

The mutual inductance is very low between the two rings of the resonator. The resonant frequency is a function of the capacitor and inductor values. The series capacitance C_S between the two rings is given in Eq. (2) [15].

$$C_s = \varepsilon\frac{at}{2g} \tag{2}$$

The value of C_s is equivalent to $C/4$. μ is the permeability of the free space, "a" the ring width, "g" the split gap, "b" the ring length, "ε" the permittivity, "t" the thickness of the material, and "l_1" the outer

length of the SRR. The dimensions of the MNG unit cell are: $a = 0.4\,\text{mm}$, $b = 2.4\,\text{mm}$, $g = 0.4\,\text{mm}$, $l_1 = 4\,\text{mm}$ and $t = 1.6\,\text{mm}$. The resonance frequency of the two-ring SRR is given in Eq. (3).

$$f = \frac{1}{2\pi\sqrt{LC_s}} \tag{3}$$

The realization of the metamaterial requires an infinite repetition of the unit element in the direction of lattice vectors. Realization requirements are fulfilled by imposing boundary conditions applied on the unit element of the metamaterial to extract the S parameter [19]. To achieve the periodicity, the structure is simulated using Ansys HFSS (A finite element method based electromagnetic solver) under PE (perfect electric) and PM (perfect magnetic) boundary conditions applied to the y-z and x-z directions when the ports are located in the y direction. The simulated S parameters of the design structure are shown in Figs. 5(a) and 5(b). Material parameters are calculated using the extracted S parameter of the SRR. The following formulas (Eqs. (4) and (5)) are used to calculate the permittivity (ε_r) and permeability (μ_r) of the material [20].

$$\varepsilon_r = \left(\frac{2}{jk_0l_1}\right)\left(\frac{1 - S_{21} - S_{11}}{1 + S_{21} + S_{11}}\right) \tag{4}$$

$$\mu_r = \left(\frac{2}{jk_0l_1}\right)\left(\frac{1 - S_{21} + S_{11}}{1 + S_{21} - S_{11}}\right) \tag{5}$$

where l_1 is the maximum length of the unit cell, and k_0 is the wave number.

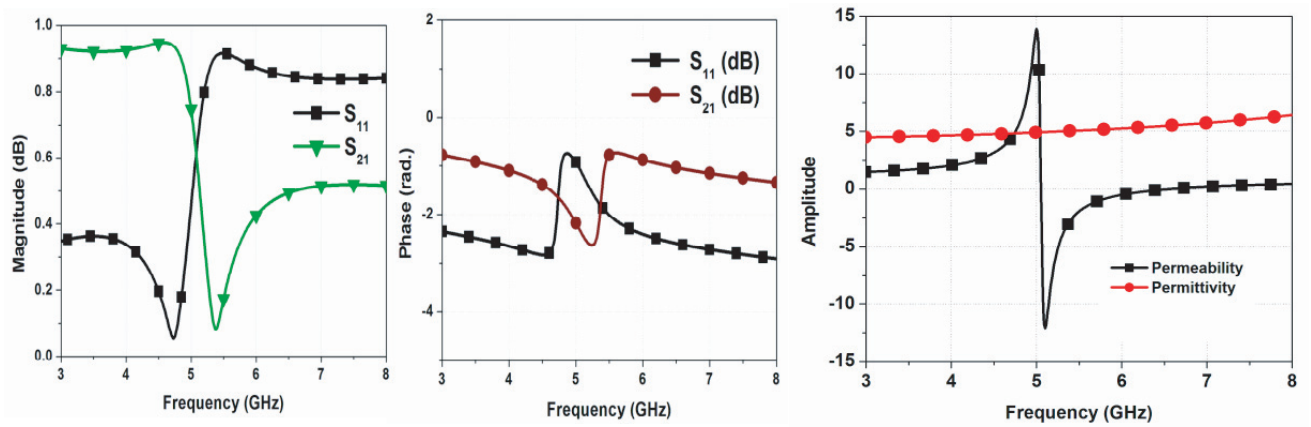

Figure 5. (a) The simulated S-parameter magnitude and (b) phase (radian) of the metamaterial unit cell and (c) extracted material parameters of the SRR unit cell.

The extracted material parameter graph, i.e., Fig. 5(c), shows that the SRR based on MNG material in the frequency range of 5 to 6 GHz.

5. ANTENNA WITH METAMATERIAL LOADING

In Antenna 1, eight SRR unit cells are integrated in the ground plane. Two unit cells are placed on the left side of the patch, and other two unit cells are placed on the right side of the patch as shown in Fig. 6. Twelve diodes are incorporated in the SRR structures as switching element to investigate the change in the radiation properties of Antenna 2. The ground plane PIN diodes are considered as D_1 to D_8. The right side of the radiator has two PIN diodes, i.e., D_9 and D_{10}, and the left side of the radiator has two PIN diodes, i.e., D_{11} and D_{12}. PIN diodes in the ground plane are connected in the same switching state, i.e., 8 PIN diodes are switched on and off at the same time. Similarly, the right (D_{11} and D_{12}) and left side (D_9 and D_{10}) PIN diodes have two distinct switching states.

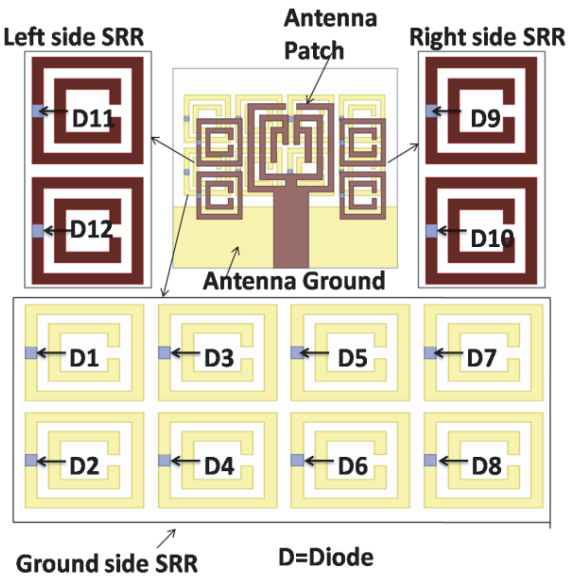

Figure 6. Antenna 2: Antenna 1 embedded with SRRs with switching combinations (8 switching stage with 12 PIN diodes).

Table 3. Different switching stages of antenna.

Switching Combination stage	Switching State 1 (diode D_{11} and D_{12})	Switching State 2 (diode D_9 and D_{10})	Switching State 3 (diode D_1 and D_8)	Frequency Spectra		Gain Max
				1st Band	2nd Band	
1	OFF	OFF	OFF	3.86–5.8	-	3.9 dB (5.39 GHz)
2	OFF	OFF	ON	3.94–5.96	-	3.7 dB (5.76 GHz)
3	OFF	ON	OFF	3.9–5.72	7.15–7.8	2.55 dB (5.48 GHz)
4	OFF	ON	ON	3.95–5.85	-	3.3 dB (5.94 GHz)
5	ON	OFF	OFF	3.92–5.98	-	4.25 dB (5.4 GHz)
6	ON	OFF	ON	4.02–6.26	-	4.67 dB (6.2 GHz)
7	ON	ON	OFF	4.02–5.81	7.2–7.8	3.2 dB (5.8 GHz)
8	ON	ON	ON	4.0–6.2	-	8.1 dB (4.9 GHz)

6. RESULT AND DISCUSSION

The gain and bandwidth also vary with different sets of the switching states. These different combinations of switching (switching stage) and corresponding simulated results in terms of bandwidth and gain are given in Table 3. The comparison of simulated S_{11} (dB) for different switching combinations stages are shown in Figs. 7(a)–7(d). In stages (1, 2, 4, 5, 6, 8), the antenna provides wide -10 dB

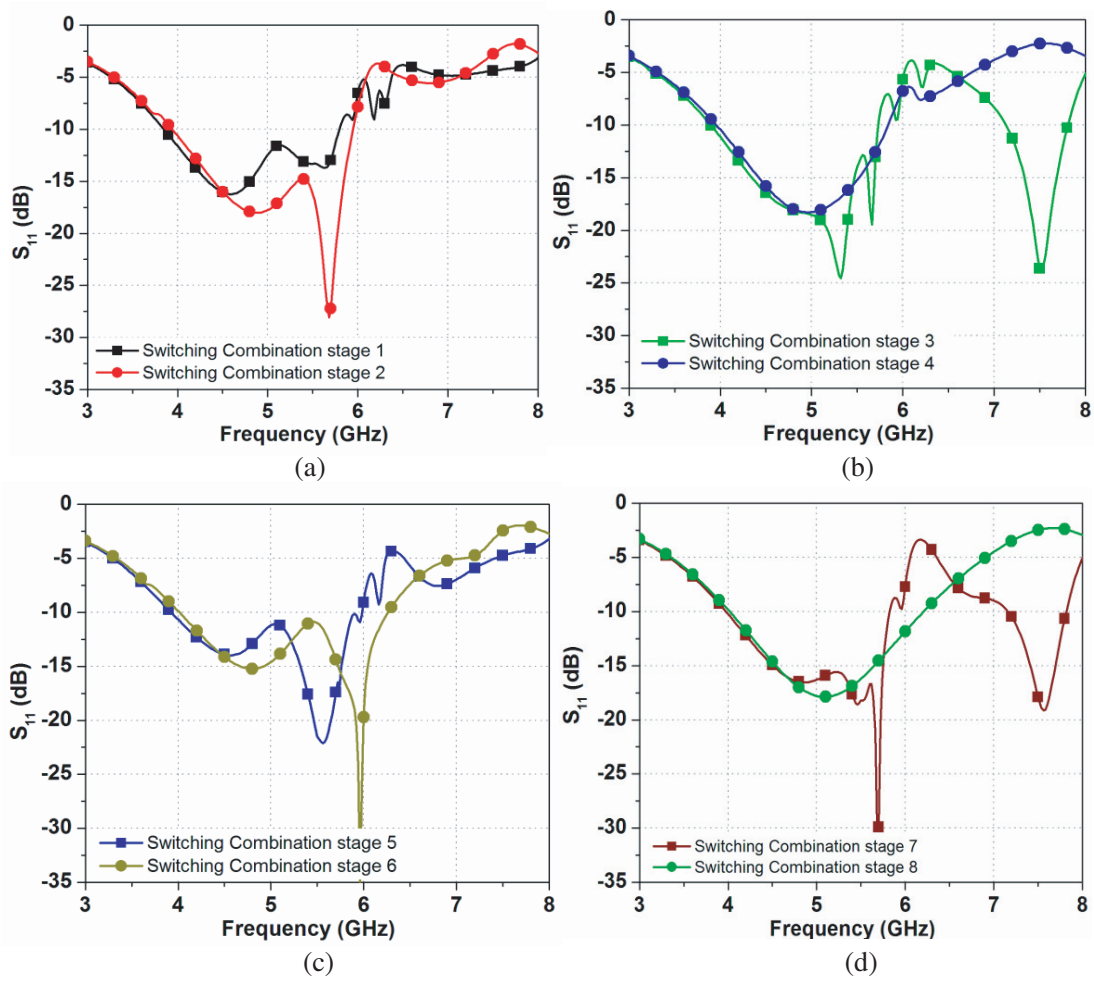

Figure 7. Simulated S_{11} parameters for different switching combinations of Antenna 2.

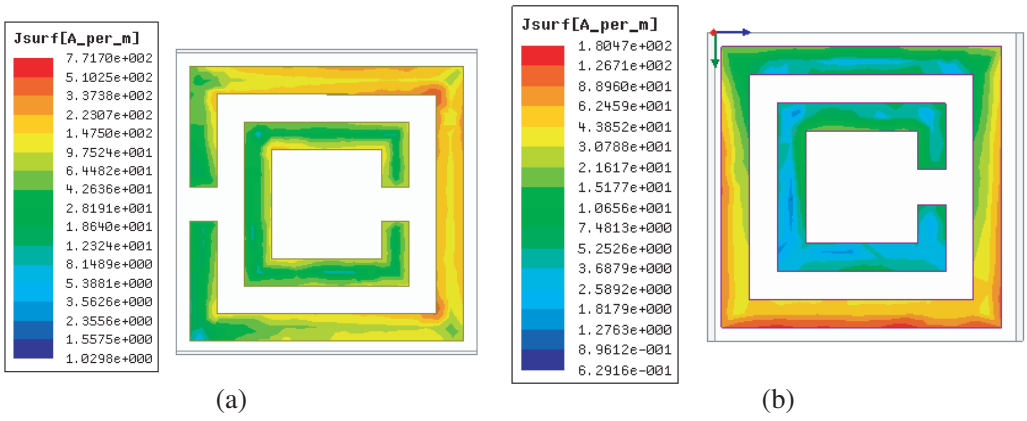

Figure 8. Current density pattern of a split ring resonator in (a) switch OFF and (b) switch ON condition.

bandwidths from 3.8 to 6 GHz. However in stages 3 and 7, the antenna provides dual-band properties in the frequency region 3 to 8 GHz.

The SRR unit cells are placed close enough to the compact antenna radiator to modify the effective permeability of the material. The current density pattern of a diode in ON and OFF in ideal condition

is shown in Figs. 8(a) and (b). It is observed that the SRR manipulates the behavior of the fringing electric fields which is caused at the end of the surface wave propagating through the patch.

The antenna radiation performance due to different switching stages and corresponding fringing field is modified. For analysing the electric field behaviour due to SRR switching, 4 different combinations of the switching stages are considered at 5.2 GHz operating frequency. The electric filed patterns of the switching stages 1, 4, 6, 8 of Antenna 2 are shown in Figs. 9(a)–9(d). The electric filed pattern of stage 1, when all diodes are in off condition, is found focused in the negative y direction as mentioned in Fig. 9(a). In stage 4 and stage 8, the electric fields are not focused in any particular direction. The fields are equally distributed in all directions of the yz plane as shown in Figs. 9(b) and 9(d). As shown

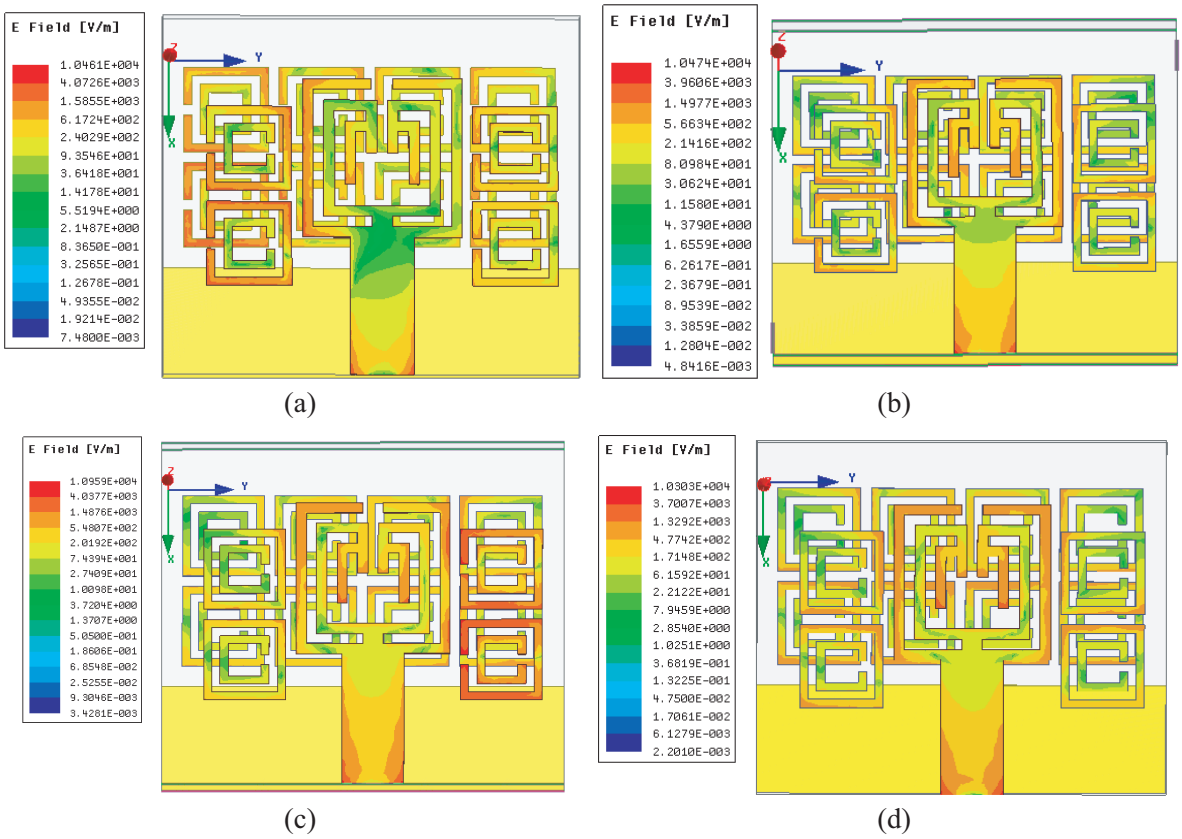

Figure 9. E field pattern of the Antenna 2 at 5.2 GHz. (a) Stage 1, (b) stage 4, (c) stage 6, and (d) stage 8.

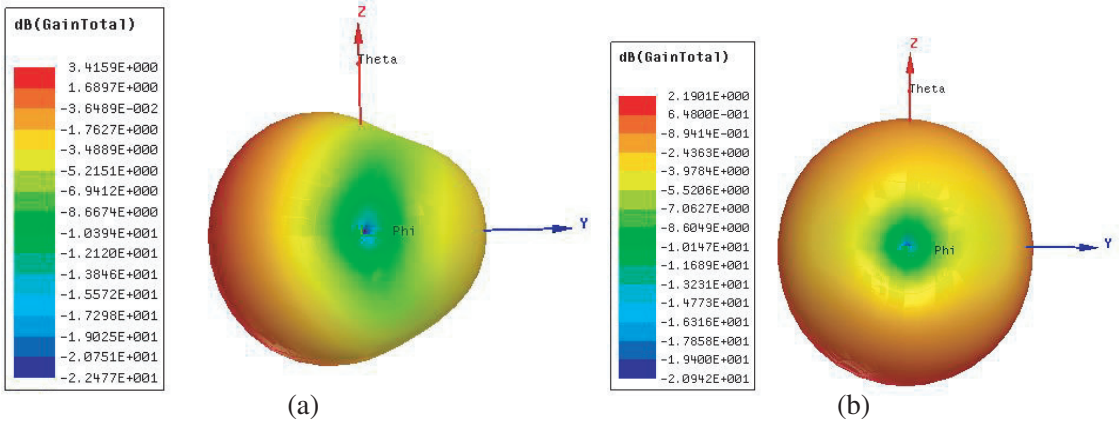

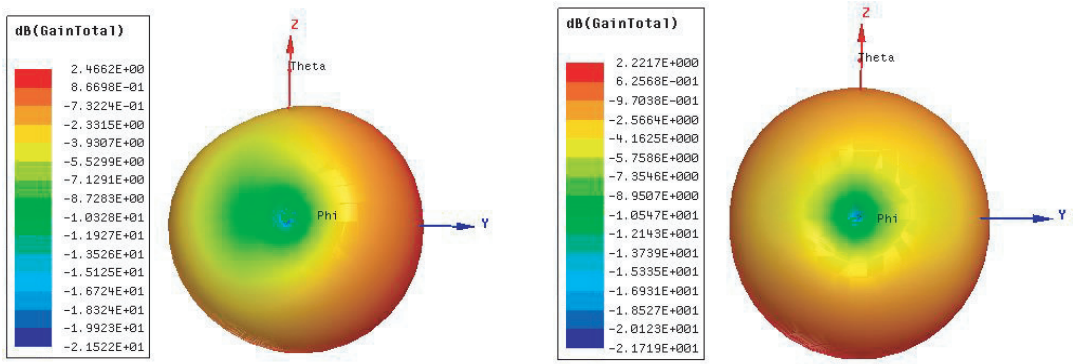

Figure 10. 3D gain radiation pattern of Antenna 2 at 5.2 GHz of (a) stage 1, (b) stage 4, (c) stage 6, and (d) stage 8.

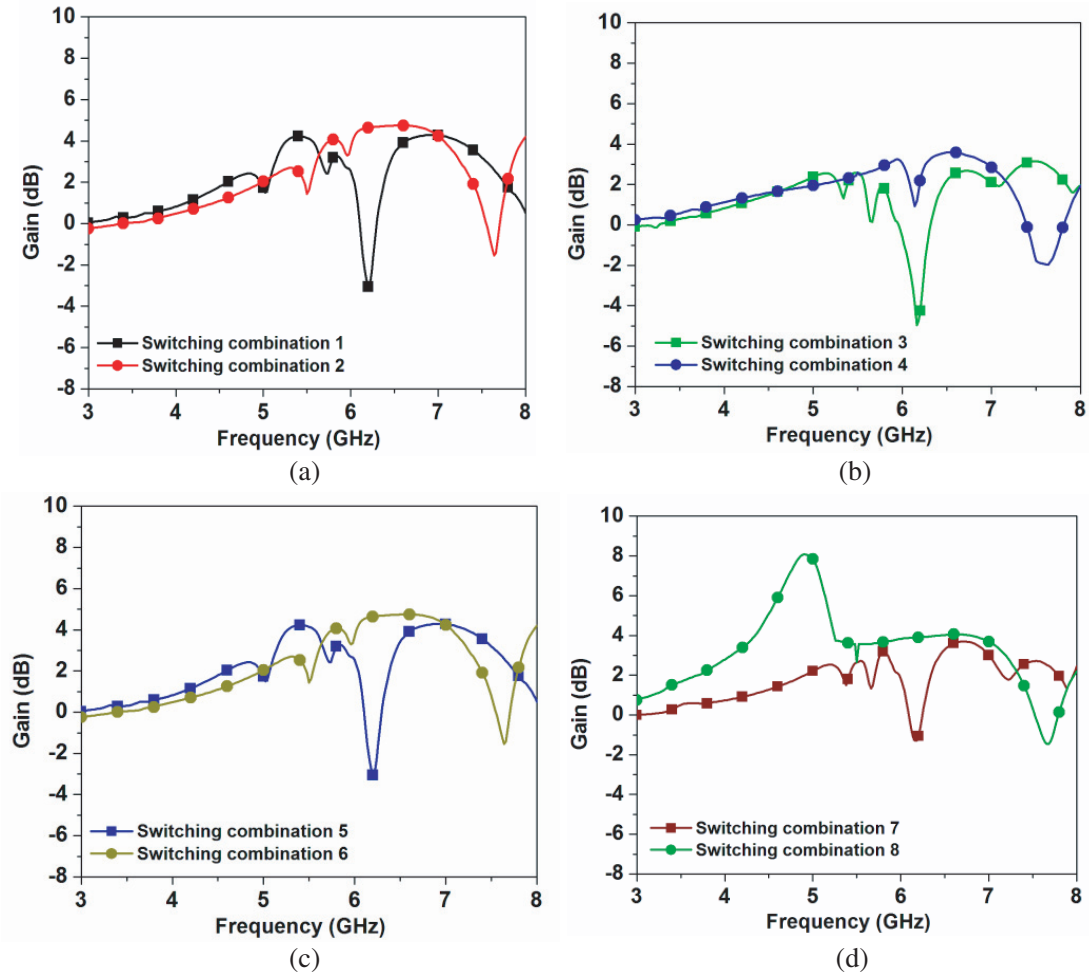

Figure 11. Simulated gain vs. frequency plot of different switching stages of Antenna 2.

in Fig. 9(c), the field is focused in positive y direction in switching stage 6. The radiation patterns associated with stages 1, 4, 6 and 8 are shown in Figs. 10(a)–10(d).

The gain vs. frequency plot of Antenna 2 in different switching combinations is shown in Fig. 11. Among all the stages, the maximum gain of 8.1 dB is achieved at 4.9 GHz in stage 8. However, the

(a) (b)

Figure 12. Fabricated prototypes (a) top (patch) and (b) bottom (ground) of Antenna 2 (considering stage 1).

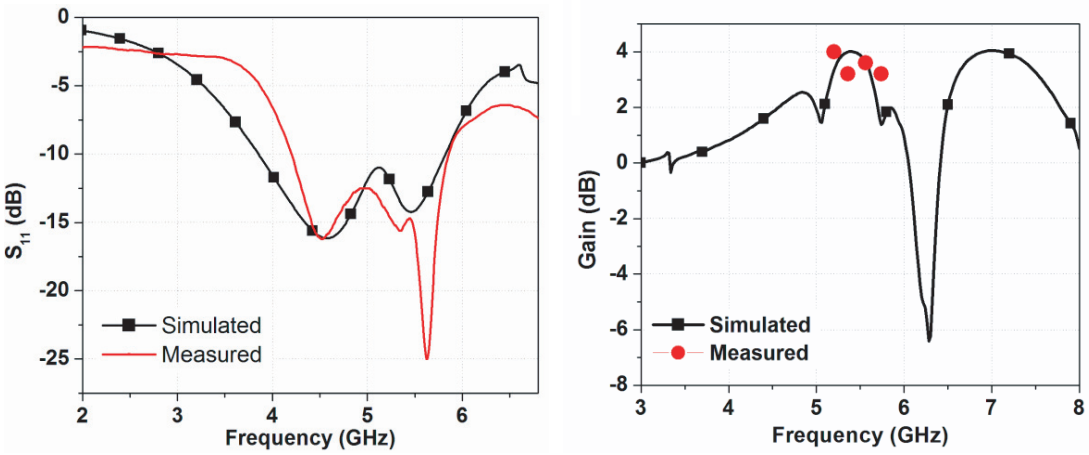

(a) (b)

Figure 13. (a) Simulated and measured S_{11} (dB) parameter switching stage 1 of Antenna 2, and (b) simulated and measured gain vs. frequency plot of switching stage 1 of Antenna 2.

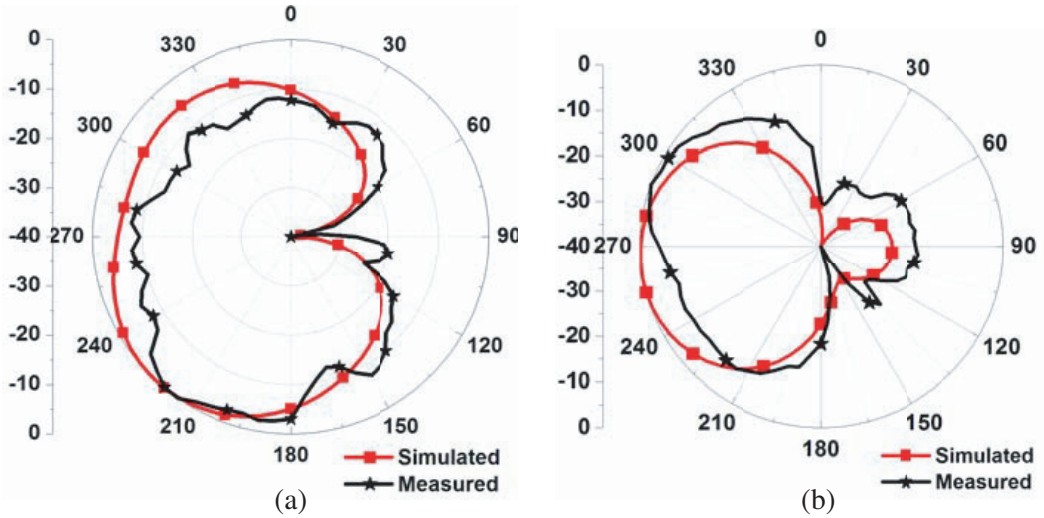

(a) (b)

Figure 14. Normalized (a) E and (b) H plane radiation pattern of the switching stage 1 of Antenna 2 at 5.2 GHz.

maximum gain of around 4 dB is achieved at 5.3 GHz (in WLAN band 5.15–5.85 GHz) in stages 1 and 5. The above analysis illustrates that the radiation performance of Antenna 2 is quite good compared to Antenna 1 due to its beam focusing capability.

The fabricated Antenna 2 with ideal diode off condition, i.e., stage 1 is shown in Figs. 12(a) and (b). The comparison graphs of simulated and measured S_{11} (dB) are shown in the Fig. 13(a), and it is found that the simulated S_{11} (dB) almost satisfies with the measurement results. The gain vs. frequency plot of the fabricated antenna is shown in Fig. 13(b), and 4 dB maximum measured gain at 5.2 GHz is found. The simulated and measured radiation patterns of Antenna 2 are shown in Fig. 14, and the measured radiation pattern shows good agreement with the simulated one.

7. CONCLUSION

Beam focusing and gain enhancement of a compact wideband microstrip antenna with Mu negative metamaterial loaded is presented in this communication. The basic and proposed antenna fulfils the bandwidth requirement of WLAN 5.2 and 5.8 GHz band and also has beam switching capability. The investigation of SRR switching results in the beam focusing and gain enhancement of the proposed antenna in different stages. The antenna radiator is compact in size by 73%. The measured -10 dB bandwidth is obtained about 31.37% (4.3 to 5.9 GHz) whereas the measured peak gain of around 4 dB is found at 5.2 GHz.

REFERENCES

1. Brown, E. R., "RF-MEMS switches for reconfigurable integrated circuits," *IEEE Trans. Microw. Theory Tech.*, Vol. 46, No. 11, 1868–1880, Nov. 1998.
2. Bai, Y.-Y., S. Xiao, M.-C. Tang, Z.-F. Ding, and B.-Z. Wang, "Wide-angle scanning phased array with pattern reconfigurable elements," *IEEE Trans. Antennas Propag.*, Vol. 59, No. 11, 4071–4076, Nov. 2011.
3. Ren, J., X. Yang, J.-Y. Yin, and Y.-Z. Yin, "A novel antenna with reconfigurable patterns using H-shaped structures," *IEEE Antennas Wireless Propag. Lett.*, Vol. 14, 915–918, Jan. 2015.
4. Akgol, O., O. Altintas, E. E. Dalkilinc, E. Unal, M. Karaaslan, and C. Sabah, "Metamaterial absorber-based multi sensor applications using a meander-line resonator," *Optical Engineering*, Vol. 56, No. 8, 087104, Aug. 2017.
5. Altintas, O., M. Aksoy, O. Akgol, E. Unal, M. Karaaslan, and C. Sabahc, "Fluid, strain and rotation sensing applications by using metamaterial based sensor," *Journal of the Electrochemical Society*, Vol. 164, No. 12, B567–B573, 2017.
6. Bakir, M., M. Karaaslan, O. Altintas, M. Bagmanci, V. Akdogan, and F. Temurtas, "Tunable energy harvesting on UHF bands especially for GSM frequencies," *International Journal of Microwave and Wireless Technologies*, 1–10, 2017.
7. Akgol, O., O. Altintas, E. Unal, M. Karaaslan, and F. Karadag, "Linear to left- and right-hand circular polarization conversion by using a metasurface structure," *International Journal of Microwave and Wireless Technologies*, 2017.
8. Altintas, O., E. Unal, O. Akgol, M. Karaaslan, F. Karadagy, and C. Sabahz, "Design of a wide band metasurface as a linear to circular polarization converter," *Modern Physics Letters B*, 2017.
9. Xu, Z. X. and W. G. Lin, "Controllable absorbing structure of metamaterial at microwave," *Progress In Electromagnetics Research*, Vol. 69, 117–125, 2007.
10. Karaaslan, M., E. Unal, E. Tetik, K. Delihacıog, F. Karadag, and F. Dincer, "Low profile antenna radiation enhancement with novel electromagnetic band gap structures," *IET Microw. Antennas Propag.*, Vol. 7, No. 3, 215–221, 2013.
11. Hwang, R.-B., H.-W. Liu, and C.-Y. Chin, "A metamaterial-based E-plane horn antenna," *Progress In Electromagnetics Research*, Vol. 93, 275–289, 2009.

12. Patel, S. K., C. Argyropoulos, and Y. P. Kosta, "Pattern controlled and frequency tunable microstrip antenna loaded with multiple split ring resonators using RF MEMS switches," DOI: 10.1049/iet-map.2017.0319.
13. Dadgarpour, A., B. Zarghooni, B. S. Virdee, and T. A. Denidni, "Beam tilting antenna using integrated metamaterial loading," *IEEE Trans. Antennas Propag.*, Vol. 62, No. 5, 2874–2879, May 2014.
14. Kim, I. and Y. Rahmat-Samii, "Electromagnetic band gap-dipole sub array antennas creating an enhanced tilted beams for future base station," *IET Microw. Antennas Propag.*, Vol. 9, No. 4, 319–327, 2015.
15. Patel, S. K. and C. Argyropoulos, "Enhanced bandwidth and gain of compact microstrip antennas loaded with multiple corrugated split ring resonators," *Journal of Electromagnetic Waves and Applications*, Vol. 30, No. 7, 945–961, 2016.
16. Rezaeieh, S. A., M. A. Antoniades, and A. M. Abbosh, "Compact wideband loop antenna partially loaded with mu-negative metamaterial unit cells for directivity enhancement," *IEEE Antennas and Wireless Propagation Letters*, Vol. 15, 1893–1896, 2016.
17. Li, D., Z. Szabó, X. Qing, E. Li, and Z. N. Chen, "A high gain antenna with an optimized metamaterial inspired superstrate," *IEEE Trans. Antennas Propag.*, Vol. 60, No. 12, 6018–6023, Dec. 2012.
18. Yu, A., F. Yang, and A. Elsherbeni, "A dual band circularly polarized ring antenna based on composite right and left handed metamaterials," *Progress In Electromagnetics Research*, Vol. 78, 73–81, 2008.
19. Numan, A. B. and M. S. Sharawi "Extraction of material parameters for metamaterials using a full-wave simulator," *IEEE Antennas Propag. Magaz.*, Vol. 55, No. 5, 202–211, Oct. 2013 (in English).
20. Ziolkowski, R. W., "Design, fabrication, and testing of double negative metamaterials," *IEEE Trans. Antennas Propag.*, Vol. 51, No. 7, 1516–1529, Jul. 2003.